ChemPubSoc
Europe

▐ Self-Assembly

Dendritic Domains with Hexagonal Symmetry Formed by X-Shaped Bolapolyphiles in Lipid Membranes

Stefan Werner,[a, c] Helgard Ebert,[a] Bob-Dan Lechner,[a] Frank Lange,[b] Anja Achilles,[b] Ruth Bärenwald,[b] Silvio Poppe,[a] Alfred Blume,[a] Kay Saalwächter,*[b] Carsten Tschierske,*[a] and Kirsten Bacia*[a, c]

Abstract: A novel class of bolapolyphile (BP) molecules are shown to integrate into phospholipid bilayers and self-assemble into unique sixfold symmetric domains of snowflake-like dendritic shapes. The BPs comprise three philicities: a lipophilic, rigid, π–π stacking core; two flexible lipophilic side chains; and two hydrophilic, hydrogen-bonding head groups. Confocal microscopy, differential scanning calorimetry, XRD, and solid-state NMR spectroscopy confirm BP-rich domains with transmembrane-oriented BPs and three to four lipid molecules per BP. Both species remain well organ-ized even above the main 1,2-dipalmitoyl-sn-glycero-3-phos-phocholine transition. The BP molecules only dissolve in the fluid membrane above 70 °C. Structural variations of the BP demonstrate that head-group hydrogen bonding is a pre-requisite for domain formation. Independent of the head group, the BPs reduce membrane corrugation. In conclusion, the BPs form nanofilaments by π stacking of aromatic cores, which reduce membrane corrugation and possibly fuse into a hexagonal network in the dendritic domains.

Introduction

Lipid membranes with their specific spatial variation of polarity along the membrane normal provide a unique environment for supramolecular structure-formation processes in two dimensions. Of particular biological relevance are, for instance, the formation of well-defined pores and channels from peptides, proteins,[1, 2] or artificial molecules,[3] and the formation of lipid domains, sometimes referred to as rafts.[4, 5] Microdomain formation and compartmentalization[6–9] are important in lending specific functions to biological membranes.[10] Synthetic

polymers, such as amphiphilic di- or triblock copolymers, often affect the membrane integrity and permeability and are, in many cases, known to form separated microdomains with specific local structure and packing,[11–13] whereas low-molecular-weight triblock molecules can stabilize bicellar structures.[14] Bipolar amphiphiles, so-called bolaamphiphiles, are incorporated into membranes to provide stabilization[15] or facilitate transbilayer diffusion.[16] Moreover, these bolaamphiphiles can operate as ligands for lectins[17] or form nanodomains.[18] Bolaamphiphiles involving molecular rods, such as octaphenylenes,[19] naphthalene or perylene diimide arrays,[20] and shorter linear biphenyl,[21] tolane,[22, 23] or polyene units,[24] provide useful scaffolds for ion or electron conductance through membranes[3] or serve as fluorescent probes.[24] Apart from these π-conjugated rods, nonconjugated linear oligospiroketals have also been incorporated into lipid membranes.[25] Although the ion transport properties, in particular, have been intensively investigated for various kinds of molecules, there is only limited knowledge about the modes of self-assembly of these synthetic molecules in membranes. This issue, which is of relevance to membrane stability and for the performance of membrane channels, could also contribute to the understanding of fundamental aspects of self-assembly in biomembranes, and is addressed herein.

Specifically, we report on a novel self-organization phenomenon of X-shaped bolapolyphiles (BPs), namely, synthetic molecules with rigid rod-like oligo(phenylene ethynylene)-based π-conjugated hydrophobic cores,[26] identical hydrophilic groups at each end, and two long aliphatic chains attached in the middle,[27–29] within lipid membranes made of 1,2-dipalmitoyl-sn-glycero-3-phosphocholine (DPPC). The unique feature is the

[a] S. Werner,+ Dr. H. Ebert,+ B.-D. Lechner,+ S. Poppe, Prof. Dr. A. Blume,
Prof. Dr. C. Tschierske, Prof. Dr. K. Bacia
Institut für Chemie, Martin-Luther-Universität Halle-Wittenberg
06120 Halle (Saale) (Germany)
E-mail: carsten.tschierske@chemie.uni-halle.de
kirsten.bacia@chemie.uni-halle.de

[b] F. Lange, A. Achilles, R. Bärenwald, Prof. Dr. K. Saalwächter
Institut für Physik - NMR
Martin-Luther-Universität Halle-Wittenberg
06120 Halle (Saale) (Germany)
E-mail: kay.saalwaechter@physik.uni-halle.de

[c] S. Werner,+ Prof. Dr. K. Bacia
ZIK HALOmem, Martin-Luther-Universität Halle-Wittenberg
06120 Halle (Saale) (Germany)

[+] These authors contributed equally to this work.

💻 Supporting information for this article is available on the WWW under
http://dx.doi.org/10.1002/chem.201405994.

self-assembly of some of these X-shaped BPs into microdomains of a clearly delineated dendritic shape with hexagonal symmetry in DPPC membranes of giant unilamellar lipid vesicles (GUVs). We used laser scanning confocal fluorescence microscopy (CFM) to image the regular dendritic domains and probe the BP orientation in these domains. To characterize the structural and dynamic features of the novel structures and correlate these with the complex phase behavior of the BP/DPPC/water system, as revealed by differential scanning calorimetry (DSC), we applied different solid-state NMR spectroscopy techniques and XRD to multilamellar vesicle (MLV) preparations.

First, the molecular design concept and syntheses of the new compounds are described, followed by CFM studies of GUVs prepared from mixtures of DPPC with each of the BPs. Next, the thermal behavior of one representative BP (**B12**) in different concentrations of mixtures of DPPC/H$_2$O studied by DSC and XRD is presented. The remainder of the paper focuses on a detailed spectroscopic characterization of **B12** in DPPC by using solid-state ^{31}P and ^{1}H NMR techniques to characterize the mobility of the respective components to explain the complex thermal behavior and investigate structural features. We conclude with a discussion of tentative structural models.

Results

Design and synthesis of materials

The structures of the investigated BPs are shown in Scheme 1. Because certain types of living organisms contain bolaamphiphilic molecules in their phospholipid membranes (albeit with different structures and without the central attachments[15, 30]),
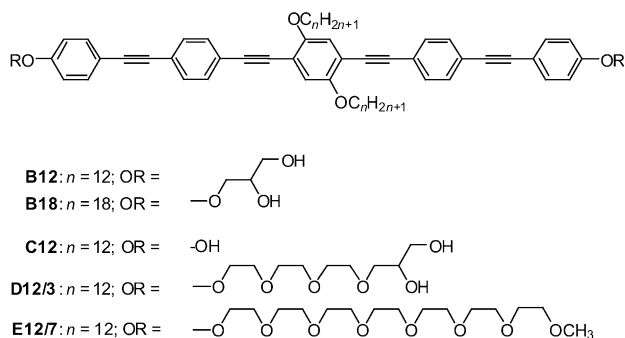
Scheme 1. Structures of the BPs **B12–E12/7**. In the nomenclature for **Bn**, **Cn**, **Dn/m**, and **En/m**, n denotes the alkyl chain length and m is the number of ethylene oxide groups.

we reasoned that X-type BPs of about 3 nm core length,[29] roughly matching the hydrophobic DPPC bilayer core, might integrate into phospholipid bilayers in a transmembrane orientation. Additional structural diversity is conveyed by the central side chains, leading to a combination of three philicities: the core is lipophilic, rigid, and capable of π–π stacking interactions; the side chains are lipophilic, but flexible; and the head groups are hydrophilic and capable of hydrogen bonding.

By using **B12** with n = 12 and glycerol head groups as a starting point and keeping the core constant, further variations were introduced: First, the length of the side chains was extended (**B18**, n = 18). In addition to side-chain variation, both glycerol head groups of **B12** were replaced by simple hydroxyl groups (**C12**), by head groups combining a hydrophilic and flexible oligo(ethylene oxide) spacer unit (EO$_3$) with glycerol moieties (**D12/3**), or by oligo(ethylene oxide) (EO$_7$) head groups incapable of acting as a hydrogen-bond donor (**E12/7**; see Scheme 1).

The polyphiles were synthesized by two strategies, as shown in Scheme 2. Compounds **Bn** (n = 12,18) with glycerol groups were obtained in a similar way to that used previously for structurally related compounds.[29] Herein, 1,2-O-isopropylidene
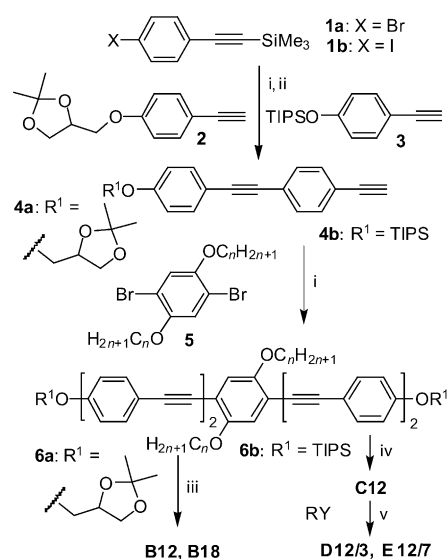
Scheme 2. Synthesis of compounds **Bn–Em/n**. Reagents and conditions: i) [Pd(PPh$_3$)$_4$], CuI, Et$_3$N, reflux, 7 h; ii) K$_2$CO$_3$, MeOH, CH$_2$Cl$_2$, RT, 10 h; iii) pyridinium tosylate (Py·TsOH), THF, MeOH, 60 °C, 5 d; iv) tetra-n-butylammonium fluoride (TBAF), THF, 25 °C, 1 h; v) K$_2$CO$_3$, DMF, 80 °C, 8 h (Y = Br and Y = OTs in the syntheses of **D12/3** and **E12/7**, respectively; R is shown in Scheme 1, TIPS = triisopropylsilyl).

glycerol substituted phenylacetylene (**2**)[31] was coupled in a Sonogashira reaction[32] with 4-bromotrimethylsilylethinylbenzene (**1a**)[33] to obtain 4′-1,2-O-isopropylideneglycerol-functionalized 4-ethinyltolane **4a** after basic cleavage (K$_2$CO$_3$/MeOH) of the C-terminal trimethylsilyl group.[34] Sonogashira coupling of **4a** (2 equiv) with 2,5-dibromohydroquinone ethers **5** (n = 12, 18)[35] led to compounds **6a** (n = 12, 18), which were deprotected with Py·TsOH in methanol[36] to give the BPs **B12** and **B18**, respectively. This last deprotection step turned out to be the bottleneck of this synthetic strategy, leading to low yields (≈20–50 %) due to the sensitivity of the electron-rich oligo(phenylene ethynylene) core under acidic conditions, the long reaction time required, and the incomplete deprotection of both glycerol groups, giving rise to purification problems. Therefore, an alternative strategy, which avoided this step, was used for the synthesis of subsequent compounds.

For the synthesis of compounds **D12/3** and **E12/7** with extended polar groups the oligo(phenylene ethynylene)-based biphenol **C12** was synthesized first in two subsequent Sonogashira coupling reactions, and the polar groups were attached in the final step through etherification reactions. In the first coupling reaction, the TIPS-protected 4-ethinylphenol **3**[37] was coupled with 4-iodophenylethinyltrimethylsilane (**1 b**)[38] to give the 4′-triisopropyloxy-substituted 4-ethyltolane **4 b** after selective base-catalyzed desilylation (K_2CO_3/MeOH) of the ethynyl group.[34] Two equivalents of **4 b** were then coupled with 2,5-dibromo-1,4-didodecyloxybenzene **5** ($n = 12$) to yield the *O*-TIPS-protected compound **6 b**. Removal of the TIPS groups under fluoride ion catalysis[39] yielded the oligo(phenylene ethynylene)-based biphenol **C12**. Etherification of **C12** with 12-bromo-3,6,9-trioxadodecane-1,2-diol (RY, Y = Br) or 3,6,9,12,15,18,21-heptaoxadocosyl-*p*-toluenesulfonate (RY, Y = OTs)[40] yielded compounds **D12/3** and **E12/7**, respectively. Analytical data and details of the syntheses and purification are described in the Supporting Information.

GUVs and CFM

GUVs represent free-standing bilayer model membranes, which, by virtue of their large size, allow direct visualization of the membrane morphology and phase separation by fluorescence microscopy. Domains with irregularly shaped boundaries are observed when a solid and a fluid membrane phase coexist, for instance, in GUVs from DPPC and 1,2-dilauroyl-*sn*-glycero-3-phosphocholine (DLPC) at room temperature.[41] In contrast, in fluid–fluid phase separation, the length of the interfacial lines becomes minimized, leading to circular domains.[42]

Electroformation, that is, rehydration of a lipid film in the presence of an alternating electric field, is a preferred method for obtaining giant vesicle preparations with a large degree of unilamellarity.[43] For the preparation of GUVs in this study, BPs were mixed with DPPC at a 1:10 molar ratio and the solvent was evaporated to yield a dry mixed film. GUVs containing both BP and phospholipid were formed upon electroformation (for details, see the Experimental Section).[44] GUVs were visualized by means of CFM by exploiting the autofluorescence of the BPs (absorption maxima at $\lambda = 334$ and 386 nm, emission maximum at $\lambda = 428$ nm) and by counterstaining with a small amount of a red fluorescent rhodamine-labeled lipid (1,2-dipalmitoyl-*sn*-glycero-phosphoethanolamine-*N*-(lissamine rhodamine B sulfonyl), Rh-PE).

GUVs from pure DPPC can only be prepared by electroformation at a temperature above the main transition temperature. When the GUVs are cooled to room temperature for CFM, the GUVs exhibit a faceted, corrugated shape and hole defects due to the presence of the gel phase,[44] as shown in Figure 1a. Next, GUVs were prepared from BPs and DPPC to test the miscibility of the two components in the membrane plane (Figure 1b–f). Incorporation of any of the BPs was found to suppress the hole defects and reduce the corrugated appearance of facetted GUVs. Some GUVs appeared smooth, whereas others were still corrugated; this was accounted for by the fact
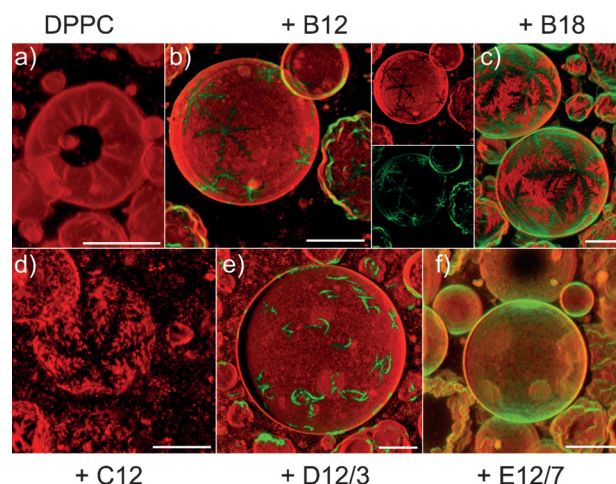

Figure 1. Confocal fluorescence images (shadow projections of axial image stacks) of GUVs from DPPC (a) and of GUVs from DPPC and different BPs (**B12** (b), **B18** (c), **C12** (d), **D12/3** (e), and **E12/7** (f)) at a 10:1 molar ratio at room temperature (22 °C). The BP autofluorescence is displayed in green. The Rh-PE counterstain is shown in red. In b), separate images for the red (Rh-PE) and green (**B12** autofluorescence) channels are also shown. In d), the BP fluorescence is not observable due to fast photobleaching of **C12**. Notably, sixfold symmetric domains with a snowflake-like appearance are observed with **B12**, **B18**, and **C12**. Scale bar = 20 μm.

that GUV samples tended to be slightly heterogeneous in quantitative compositions.[45] Most notably, the domains formed by **B12** had a striking, snowflake-like appearance, which featured sixfold symmetry and dendritic branches (Figure 1b). The dendritic domains are probably formed through a kinetically controlled nucleation and growth mechanism[46] and bear a superficial resemblance to phase-separated structures observed in mixed-lipid GUVs[10] or supported bilayers.[6,7] The clean sixfold symmetry observed for **B12** is remarkable. It suggests a regular packing structure of the BP and lipid components, and most likely reflects its local symmetry.

Chemical variations allow us to delineate necessary conditions for the formation of the observed domains. A similar, sixfold-symmetric snowflake-like appearance to that of **B12** was observed for **B18** (Figure 1c), which was a polyphile with extended lateral alkyl chains, as well as with **C12**, which represented a polyphile with only a single hydroxyl head group at each end (Figure 1d). A bulkier head group (**D12/3**), which combines the glycerol moiety with an (EO)₃ spacer unit, preserves phase separation into domains, but removes the strict symmetry, resulting in boomerang-shaped domains (Figure 1e). Only **E12/7**, which carries methoxy-terminated (EO)₇ head groups that are incapable of acting as a hydrogen-bond donor, does not form macroscopically segregated domains. The nearly uniformly distributed green fluorescence indicates that, in this case, individual BPs or small microdomains are randomly distributed in the lipid bilayer. Hence, the ability of the polyphiles to form hydrogen bonds appears to be a prerequisite for macroscopic segregation. Enlargement and increased flexibility of the head groups appear to contribute to a reduced size and regularity of the domains.

The characteristic angle dependence of the fluorescence intensity along the perimeter of a macroscopically homogeneous
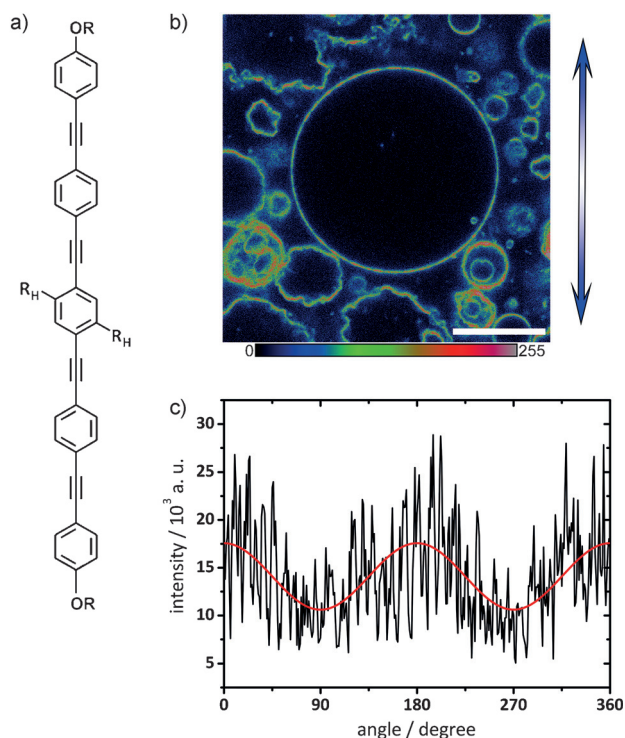
Figure 2. a) Structure of the BP core (substituents OR as in Scheme 1 and $R_H = OC_{12}H_{25}$). b) Confocal slice of GUVs prepared from a 1:10 ratio of **E12/7** and DPPC, excited with polarized $\lambda = 405$ nm laser light. The direction of polarization is indicated by the blue double arrow. A multicolor palette (as depicted below) is used to highlight fluorescence intensity variations. Scale bar = 20 μm. Imaging was performed at room temperature (22 °C). c) The fluorescence intensity along the perimeter of the largest GUV in b) as a function of angle γ (black line: data; red line: cosine-squared fit function, $I = a + b\cos^2(\gamma)$) shows maxima at the top and bottom of the image and minima to the right and the left; this indicates an approximately transmembrane incorporation of the BP into the bilayer.

GUV, illuminated with linearly polarized light, is indicative of the orientation of a fluorophore in a bilayer membrane.[47–49] Therefore, BP fluorescence along the perimeter of the GUVs obtained by confocal laser scanning microscopy with a polarized laser beam was used to study how the BP was incorporated into the membrane. A single confocal slice of the GUVs containing **E12/7** from Figure 1 f is shown in Figure 2. The transition dipole moment of BP is approximately parallel to the long axis of the rod-like aromatic core. The systematic variation in fluorescence intensity along the perimeter of a GUV with fluorescence maxima appearing at the top and bottom of the microscope image and minima appearing to the right and left confirms that the BP is indeed integrated into the phospholipid bilayer in an approximately transmembrane orientation. The pronounced noise-like fluctuations suggest that GUVs from the 1:10 mixture of **E12/7** and DPPC are not perfectly homogeneous, but heterogeneous around the confocal resolution limit.

DSC investigation of B12/DPPC mixtures

To obtain a better understanding of the origin of the unusual mode of molecular self-assembly in the lipid layers, in-depth investigations of **B12**/DPPC mixtures were performed. DPPC
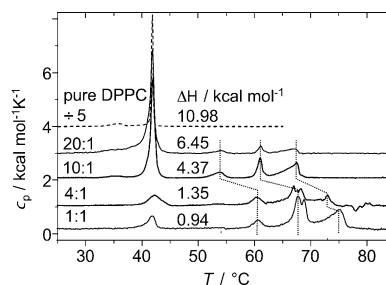

Figure 3. DSC thermograms of MLV preparations of pure DPPC and of **B12** in mixtures with DPPC with different molar ratios. The indicated ΔH values refer to the sum of the pre- and main transition of DPPC in units of kcal mol^{-1} lipid.

forms a gel phase at room temperature, and the DSC results shown in Figure 3 demonstrate a reduced transition enthalpy for the main lipid gel to fluid phase transition at 42 °C upon mixing with increasing amounts of **B12**. Three new transitions appear between 50 and 70 °C, which suggests the existence of phase separation within the membrane. The whole set of three new transitions shifts to higher temperature for a DPPC/**B12** ratio of 4:1 and lower, which indicates a change in the composition of the domains with increasing **B12** content. The reduced ΔH values for the main transition at 42 °C suggest that a significant fraction of lipid molecules do not take part in the main transition at this temperature, but become disordered only at higher temperature. The sum of all peak areas in the mixtures remains almost constant, which indicates that at 80 °C all DPPC molecules are in the disordered state. Because the length of the domain boundaries in a phase-separated system can also decrease the transition enthalpies, we refrain from a quantitative interpretation of the reduced ΔH values, and refer to our NMR spectroscopy based assessment described below.

XRD investigation of a B12/DPPC mixture

The phase behavior and demixing phenomena found by DSC were also investigated by using temperature-dependent powder XRD to gain more insight into the structural organization of the **B12**/DPPC system as a function of temperature. A **B12**/DPPC sample with a molar mixing ratio of 1:10 was prepared within a capillary and temperature-dependent powder patterns were recorded (Figure 4). In the SAXS region, up to four reflections with equidistant positions are visible, which indicate the presence of a lamellar structure. The WAXS region shows two strong reflections: the (020) and (110) reflections from the chain lattice of the lipids. From these reflections, the chain packing mode and tilt angle of the chains can be determined to be similar to pure DPPC.

The repeat distance (membrane plus interlamellar water layer thickness) within the multilayer stacks was determined at different temperatures. At room temperature, the lamellar repeat distance of the mixture is slightly larger (d (1:10) = 7.25 nm) than the distance found for pure DPPC bilayers (d = 6.35 nm at 20 °C in the $L_{\beta'}$ phase and 6.70 nm at 50 °C in the L_α phase).[50] The interlamellar water layers are thus increased in

B12:DPPC 1:10 in H₂O (50 wt.%)

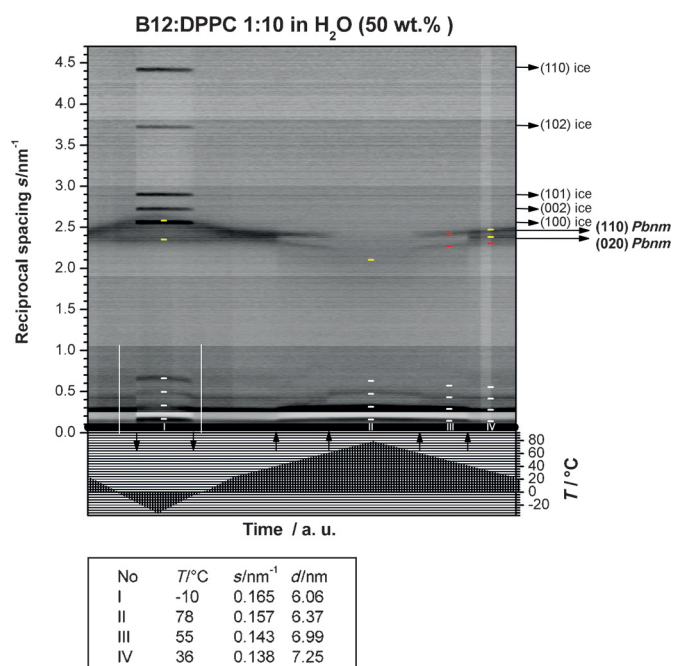| No	T/°C	s/nm^{-1}	d/nm
I	−10	0.165	6.06
II	78	0.157	6.37
III	55	0.143	6.99
IV	36	0.138	7.25

Figure 4. X-ray contour plot of aqueous suspensions of **B12**/DPPC (1:10) with 50 wt % H₂O. In the upper part, the scattering intensities are plotted in grayscales (reciprocal spacing axis at the left-hand side) and the temperature profile is plotted in the lower part (temperature axis at the lower right-hand side). Arrows pointing upwards mark phase transitions, and arrows pointing downwards show the freezing and melting of excess water. Scattering curves at 0 °C are highlighted with white vertical lines. At temperatures between the freezing and melting of water, sharp ice reflections appear that are indexed with horizontal arrows in the right-hand border. Small-angle X-ray scattering (SAXS) reflections at temperatures I–IV are marked with white horizontal dashes and respective reflections of the wide-angle X-ray scattering (WAXS) region with yellow or red dashes (two phases). The WAXS reflection indexing in the right-hand border (long horizontal arrows) refers to the lipid-rich phase. The box at the bottom shows the repeat distances at the marked temperatures (I–IV).

thickness and/or the molecular tilt has decreased. An increase in the water layer thickness can be caused by a change in hydration of the head-group region due to the incorporation of the **B12** molecules, which, at the same time, can also induce a reduction of the tilt angle of the lipid chains. For a phase-separated system, we would expect two sets of lamellar repeat distances in the SAXS region, provided that the phase-separated domains do not have identical thicknesses of lipid layers including the water layer. Analysis of the profiles of the peaks in the SAXS region indicate only that the peaks may have a shoulder. Experiments that have been performed on oriented bilayers by using X-ray reflectometry support this finding because the shoulders are more pronounced.[51] In addition, at a higher temperature of approximately 50 °C, when the lipids in the almost pure DPPC domains are fluid, the difference in layer thickness between the two domain types becomes larger and the two sets of SAXS reflections are more clearly separated.

In the WAXS region, the reciprocal spacings of 2.33 (110) and 2.43 nm^{-1} (020) indicate the presence of an orthorhombic (symmetry group *Pbnm*) herringbone lattice[52] with tilted chains characteristic for bilayers in an L$_{\beta'}$ phase at room tem-

perature. Upon cooling below room temperature, an increase in splitting of the two WAXS reflections is observed, which indicates a further change in chain packing. When the sample is further cooled below 0 °C, the crystallization of excess water leads to the appearance of sharp ice reflections. The freezing of interlamellar water leads to reduced membrane repeat distances ($d = 6.06$ nm). After heating the sample again to room temperature, the initial repeat distance, and thus, the membrane structure is restored, which indicates a reversible process of excess water freezing (dehydration/hydration).

At higher temperatures, the two WAXS reflections change into a broad scattering peak, which indicates the transition from the gel to the fluid L$_\alpha$ phase. For the 1:10 mixture, this occurs at 42 °C in coincidence with the main transition at T_m observed by DSC. Above this transition, still intense WAXS peaks are visible at slightly different reciprocal spacings and additional WAXS peaks appear ($s_{T>42°C} = 2.25$ and 2.39 nm^{-1}). These reflections indicate that the sample still contains some ordered lipid chains, but the packing is in a different geometry to that of the normal L$_{\beta'}$-phase with tilted chains.

Above 68 °C, fluid high-temperature phases are formed. No sharp reflections, but only a broad halo characteristic for fluid chains is visible in the WAXS region. The layer thickness is further decreased, as expected for a fluid lipid bilayer (d (1:10) = 6.37 nm), and the high-temperature fluid phase appears to be homogeneously mixed.

The XRD results support the assumptions based on the DSC results that the mixtures seem to be phase separated. The XRD results clearly show that a pure or very DPPC-rich lamellar phase must exist, which transforms into a fluid L$_\alpha$ phase at a temperature of 42 °C. Above this temperature, part of the lipids are still ordered and probably form a type of complex with **B12**, in which the chains are in a different chain lattice. A homogeneous fluid phase is only formed at very high temperature above 68 °C with a reduced lamellar repeat distance and a typical broad halo in the WAXS region that is characteristic for fluid chains. The X-ray results for the **B12**/DPPC (1:4) mixture are similar (not shown), although the phase separation at low temperature is not as pronounced. This is also evident in the DSC curves, in which the low-temperature transition peak characteristic for DPPC is much smaller.

NMR spectroscopy of B12/DPPC mixtures

Information on the physical properties of the membranes and changes associated with the addition of **B12** can be obtained by static ^{31}P NMR spectroscopy. The single ^{31}P nucleus in the lipid head group has a strongly orientation-dependent chemical shift (chemical-shift anisotropy (CSA)), which is sensitive to rotational motions of the head group.[53, 54] The width of the CSA tensor, $\Delta\nu$, is preaveraged by fast axial rotations, leading to a symmetric tensor with a principal axis parallel to the membrane normal. The extent of rotational averaging depends on the mobility of the lipid and primarily reflects the phase state, that is, the more confined environment of the gel phase and the more mobile environment of the fluid L$_\alpha$ phase. This is demonstrated for experimental results on pure DPPC given in
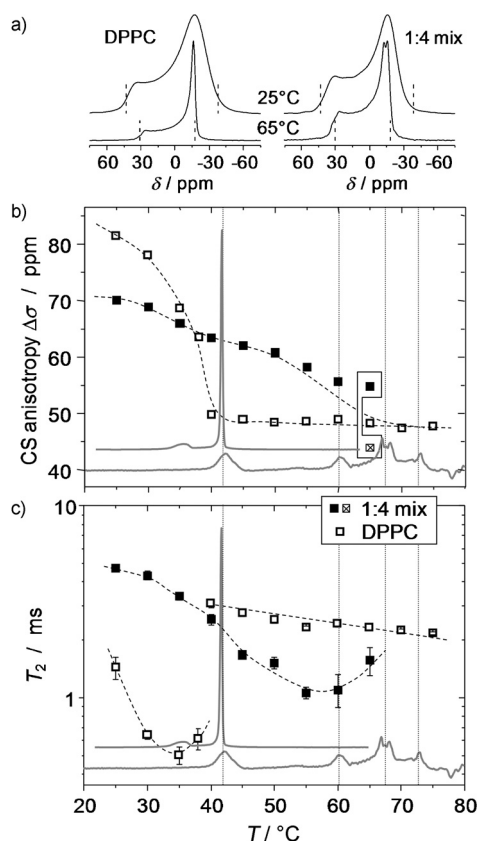
Figure 5. ^{31}P NMR spectroscopy of a 1:4 mixture of **B12** with DPPC and of pure DPPC. a) Static spectra reflecting the CSA of the ^{31}P of DPPC in the L$_\alpha$ phase (47 ppm or 7.6 kHz between the dashed lines) and in the gel phase (81 ppm or 13.1 kHz) of the pure lipid (left) and corresponding data for the mixture (right). b) CSA values as a function of temperature. c) ^{13}P T_2 relaxation times evaluated at the magic-angle orientation (around $\delta = 0$ ppm in the spectra); the minimum arises from slow lipid rotations in the gel phase. The slight temperature shifts of the NMR spectroscopy data relative to the DSC traces (gray in the background) originate from weak radiofrequency-induced heating due to ^{1}H decoupling and possible errors in the temperature calibration.

Figure 5 a and b, which show the well-documented spectral changes.[54]

Qualitative changes are observed for the spectra of the 1:4 mixture (Figure 5 a, right column, and b). In lieu of the steep pretransitional drop to a lower CSA value above 40 °C, $\Delta\sigma$ in the mixture exhibits a decay with indications of a two-step feature associated with the reduced main transition and the first new transition in DSC. This is the first indication that a fraction of DPPC is still within the gel phase above 40 °C, as further substantiated below. Notably, the $\Delta\sigma$ values represent an average over the different DPPC fractions, that is, the one associated with **B12** still in the gel phase and the mobilized fraction. The intrinsic line width of the spectra is only sufficiently reduced at 65 °C, so that the two fractions can be discriminated (see the connected points in Figure 5 b). The fact that the $\Delta\sigma$ value associated with the L$_\alpha$ phase falls below the bulk value can be attributed to the inaccuracy related to the simple reading off of the anisotropy values, which is ambiguous due to the intrinsic line width. An important observation at low temperatures is that the $\Delta\sigma$ value of the mixture is lower than that

for pure DPPC. This $\Delta\sigma$ value is, of course, an average of two components, but it indicates that the second fraction of immobilized lipid displays larger-amplitude, fast head-group fluctuations than a pure DPPC gel phase. This is in agreement with the WAXS observations, which indicate a lattice that is different from the normal L$_\beta$-phase.

The intrinsic line broadening (refocused line width) is best studied by Hahn-echo T_2 relaxation time measurements, the results of which are shown in Figure 5 c. The T_2 decay was evaluated at the isotropic-shift position of the CSA patterns (center of gravity, close to $\delta = 0$ ppm), corresponding to the magic-angle orientation of the membrane normal in the vesicle preparations with respect to the magnetic field B_0, in which T_2 is sensitive to slow orientation fluctuations. The minimum in the gel phase arises from the onset of free-lipid rotation on a timescale of $(\Delta\sigma\nu_l)^{-1} \approx 0.1$ ms, whereas the slow decay in the fluid phase is associated with slower bending modes.[54] Again expectedly, the lower average T_2 value in the mixture reflects intermediate behavior, for which the minimum of the unmodified DPPC fraction is barely visible. The most important effect is the shifted minimum, which demonstrates that the larger part of the lipid is still in a gel phase above 40 °C. Clearly, the T_2 value of the mixed system approaches the bulk value only at temperatures above 75 °C, at which **B12** is freely mobile in the membrane. The latter can be demonstrated with the help of quantitative ^{1}H NMR spectra, which we now discuss.

Quantitative temperature-dependent magic-angle spinning (MAS) ^{1}H NMR spectra were taken to first quantify the amount of lipid involved in the different phases, by taking advantage of the fact that the aliphatic lipid resonances associated with the ordered gel phase are broadened by strong ^{1}H–^{1}H dipole–dipole couplings beyond detection at moderate MAS, namely, 5 kHz spinning frequency (Figure 6 a). Integrations of the aliphatic and glycerol (C$_2$ proton) resonances (Figure 6 b) reveal that, for the 4:1 and 10:1 mixtures, only around 10–15 and 50–55 %, respectively, of the total expected signal is visible above the transition into the fluid L$_\alpha$ phase at 42 °C. This suggests that significant amounts of DPPC do not participate in this transition, but are associated with a rather immobile **B12**-rich phase. Taking into account the contribution of **B12** residues to the two signal regions, we consistently estimate the mixed phase to be composed of about 3.4 and 4.2 immobilized DPPC molecules per **B12** molecule for the 4:1 and 10:1 mixtures, respectively.

Figure 6 b also demonstrates that, within the error margin of about 20 % intrinsic to our comparison of different samples, all resonances are visible in the MAS ^{1}H NMR spectrum above 75 °C. Thus, the aliphatic chains of all membrane components, as well as the **B12** aromatic cores seen at $\delta \approx 7$ ppm, are completely mobilized and possibly dissolved in a homogeneous membrane above the last transition. As determined from the inflection points of the sigmoidal trends, the majority of the still immobilized DPPC tails are consistently seen to become mobile about 5 °C below the **B12** cores. Thus, the two highest DSC transitions are assigned to DPPC melting and **B12** melting/dissolution, respectively, which confirms the interpretation of the ^{31}P NMR spectroscopy data of the head group.
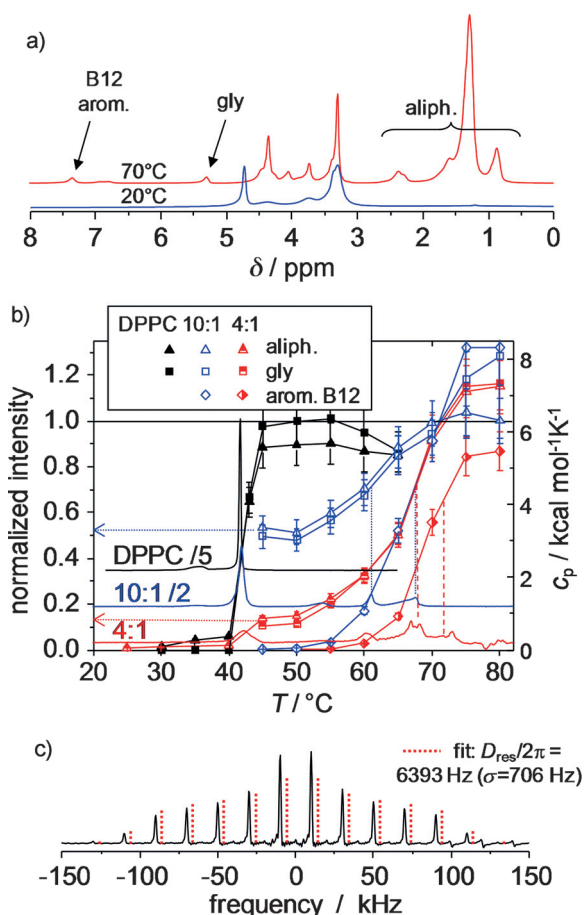
Figure 6. MAS ^{1}H NMR data (5 kHz spinning) of hydrated pure DPPC and DPPC/**B12** MLV preparations. a) Exemplary quantitative ^{1}H NMR spectra of a 4:1 mixture obtained by using a recycle delay of 8 s at 20 and 70 °C. b) Integrals of different spectral regions, normalized to 100 % as the total expected signal, as a function of temperature overlaid with scaled DSC traces (right vertical scale) and c) double-quantum (DQ) spinning sideband pattern (10 kHz MAS) for the aromatic **B12** resonance of a 4:1 mixture at 75 °C by using the BaBa-xy16 pulse sequence[55] with a recoupling time of 4 rotor periods.

Details on the dynamic state (amplitude of motion) and orientation of **B12** can be inferred from the dynamic order parameter, S, associated with different internuclear vectors. It can be probed by suitable NMR spectroscopy techniques that measure the respective residual (motion-averaged) dipole–dipole coupling constants, D_{res},[56] by using $S = D_{res}/D_{stat}$, in which D_{stat} is the effective static-limit coupling constant in rad s⁻¹. Specifically, fast orientation fluctuations (which are much faster than $1/D_{stat}$) of dissolved **B12** can be characterized by the [1]H–[1]H dipole–dipole coupling of pairs of neighboring aromatic protons to exploit the fact that the internuclear vector points along the long axis and is thus not affected by fast uniaxial rotation. The value of D_{res} can be obtained from DQ[57] spinning sideband analysis.[58] From the result at 75 °C (Figure 6 c), in combination with a reference coupling, $D_{stat}/2\pi$, of 8.2 kHz, which corresponds to an H–H distance of 2.45 Å, we obtain $S = 0.78 \pm 0.1$, which characterizes orientation fluctuations of the **B12** long axis. This can be interpreted by models that assume diffusive motion of the long axis on or within a cone

with half-opening angles of 20 or 30°, respectively. This reinforces the conclusion of a mainly transmembrane orientation of **B12** already inferred from the fluorescence measurements at lower temperature.

For further refinement of the analysis, we use advanced ^{13}C–^{1}H dipolar solid-state NMR spectroscopy techniques.[56] An account of these results is beyond the scope of this work and will be reported separately. To summarize, similar [13]C–[1]H order parameter measurements unambiguously demonstrate that **B12** performs fast, well-defined 180° flip motions in DPPC MLVs at room temperature, as well as in its pure, crystalline state. This is a common process for p-substituted, π–π-stacked phenyl rings.[59] In contrast, above all thermal transitions in the miscible phase (75 °C), the data confirm free rotation of **B12**.

The π–π interactions between aromatic rings are corroborated by our observation of a redshifted fluorescence of **B12** in the star-shaped domains of DPPC GUVs, when visualized with a spectral detector, compared with **B12** dissolved in organic solvent (Figure 7). This redshift of the fluorescence due to π–π interactions is also observed in fluorescence spectra of MLVs taken at 20 °C, at which the emission observed for **B12** in solution becomes shifted to longer wavelength when incorporated into DPPC bilayers. Above the transition at 75 °C, the fluorescence spectrum becomes nearly identical to that recorded in solution in chloroform; this indicates that the **B12** molecules are now molecularly dispersed in the bilayers.[51]

We finally note that ^{1}H MAS spectra were also recorded for an MLV mixture of DPPC and **E12/7** (see Scheme 1). Here, a very gradual mobilization of the **E12/7** aromatic cores is also only seen above the main DPPC phase-transition temperature, which indicates that, in this case, when no macroscopic domain formation was observed optically (see Figure 1 f), π-stacked, rigid aggregates should also be present. Apparently, these aggregates form microdomains that randomly pervade the DPPC membranes, smooth out the GUV membranes, and explain that the majority of giant vesicles lack visible corrugation.

Discussion

Based on these insights, we discuss tentative models of self-assembly of the X-shaped BPs in the lipid bilayers. XRD investigations and DSC results indicate that the **B12**/DPPC mixtures are phase separated. The major phase is a pure or very DPPC-rich lamellar $L_{\beta'}$ phase, which transforms into a fluid L_α phase at a temperature of 42 °C. The **B12** molecules self-assemble into **B12**-rich domains that contain highly ordered, tightly π–π-stacked **B12** molecules oriented, on average, along the membrane normal and are only able to perform π flips. In the **B12**-rich domains, about 3–4 DPPC molecules per **B12** molecule are involved, which display enhanced head-group mobility, although the chain order (probably on a different lattice) is retained even above 42 °C, that is, the chains appear to be immobilized.

At first sight, a simple explanation for the dendritic appearance of the **B12**-enriched domains in the confocal images of GUV membranes (Figure 1 b) might seem to be defect lines
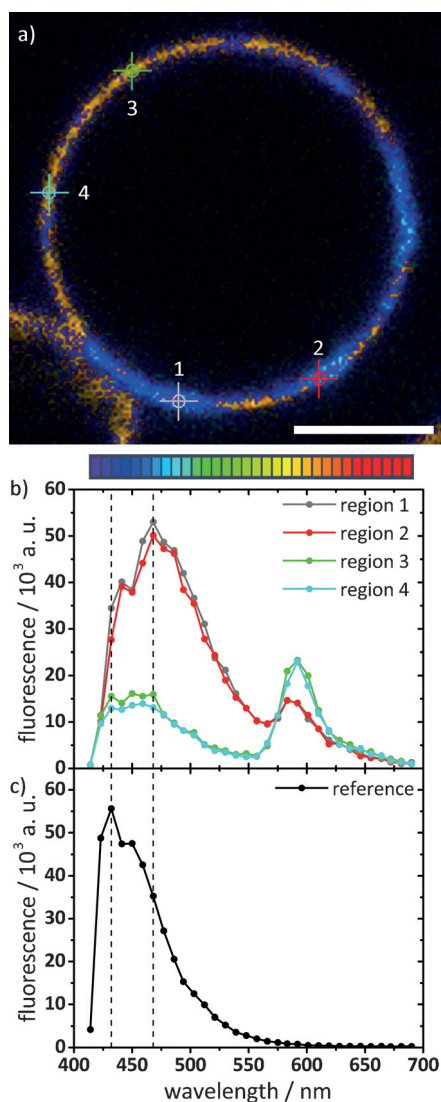
Figure 7. Spectrally resolved CFM of GUVs from **B12**/DPPC (1:10), counterstained with Rh-PE. a) Confocal slice image color-coded by wavelength, as indicated by the color palette below (32 channels, $\lambda = 414$ to 690 nm, 8.9 nm resolution). Scale bar $= 5$ µm. Imaging was performed at room temperature. b) Corresponding spectral plots for the four regions indicated by circles in the confocal image. Regions 1 and 2 are located in the **B12**-rich star-shaped domains; regions 3 and 4 are in the surrounding phase. The peak at $\lambda \approx 470$ nm (which is higher within the domains) is due to **B12** emission; the peak at $\lambda \approx 590$ nm (which is higher outside the domains) is due to Rh-PE emission. c) As a reference, the spectrally resolved fluorescence of **B12** in chloroform/methanol was recorded on the same setup, and showed a peak at $\lambda \approx 430$ nm.

around the gel-phase facets formed upon cooling and gel-phase formation in DPPC GUVs. One might envision that these may be occupied by the **B12**-enriched domains. However, if this were the case, an irregular network of **B12**-filled cracks would be expected to cover the surface of the GUVs, instead of the impressively regular, hexagonal, star-shaped domains observed in the **B12**, **B18**, and **C12** samples.

It could also be envisaged that, according to the solid docks hypothesis,[9] the BP microdomains favor chain crystallization of the lipid molecules around them, as indicated by the observed increase in the transition temperature to the fluid L_α

phase of DPPCs associated with the BPs. The simultaneously enhanced head-group mobility of these immobilized lipids suggests that the orthorhombic chain packing might be modified. The observed dendritic growth of the domains with hexagonal symmetry could result if the symmetry of chain packing were changed to hexagonal in the BP-rich domains, at least in time and space average.

Our observation of well-packed BPs with motions restricted to π flips suggests that they form extended filaments with parallel π faces. An analogous filament formation has recently been demonstrated for bolaamphiphiles without lateral chains in the absence of lipids.[60] With the X-shaped bolaamphiles used herein, the additional lateral alkyl chains interact and preferentially mix with the alkyl chains of the DPPC molecules; thus separating adjacent BP filaments. Moreover, the BP head groups capable of hydrogen bonding are expected to additionally stabilize the string-like filaments. The strings may become interconnected, resulting in a random network. The lack of visible corrugation in the DPPC-rich parts of the GUVs could be explained by a low density of randomly distributed nanofilaments that smooth out and stabilize the membranes by gluing together larger patches of DPPC gel phase. The six-fold symmetric shape of the **B12**-rich domains could, in this case, result from a fusion of these filaments into a regular hexagonal net. A tentative model that takes into consideration all these restrictions, in which the walls are built of transmembrane-oriented, aligned, and π–π-packed **B12** cores, is shown in Figure 8 and in the Supporting Information. The resulting hexagonal cells are filled by the lateral chains of the **B12** and DPPC molecules that become immobilized by this confinement. As the overall effective head group to chain cross-sectional area ratio of the superstructure is reduced (by the lateral chains of BP and the smaller head groups of most BPs), lipid-chain immobilization could indeed be associated with the observed lipid head-group mobilization. Based on the maximum observed ratio for **B12**/DPPC of around 1:3 (**B12**-rich domains) and considering the dimensions of the involved molecules, it is estimated that at least 7 molecules of **B12** are arranged along
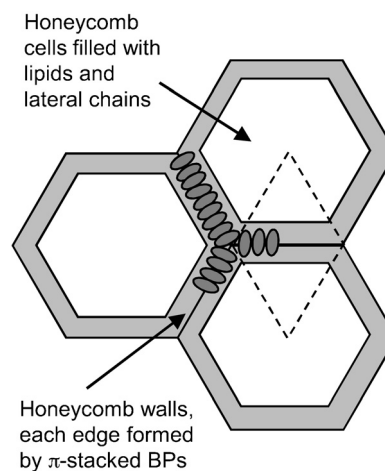

Figure 8. Model showing the organization of BPs (**B12**) in a hexagonal honeycomb (cut perpendicular to the membrane normal).

each of the honeycomb walls; thus accommodating about 50 DPPC molecules in the hexagonal cells, as estimated by calculations given in the Supporting Information. This dense packing in hexagonal honeycombs could be favored by hydrogen bonding between the relatively small head groups of the BPs **B12**, **B18**, and **C12**, whereas larger head groups with reduced capability for hydrogen bonding cannot fuse to form a dense honeycomb, and thus, the BP filaments remain randomly distributed in the lipid matrix, as observed for **E12/7**.

The formation of polygonal honeycombs composed of parallel aligned aromatic cores is a common feature of BPs, previously found as a dominating mode of self-assembly of such molecules in liquid-crystalline (LC) bulk phases.[27–29,61] However, in contrast to most reported LC honeycombs with aromatic cores oriented tangentially around the lipophilic domains, in the membranes, as a result of the confinement provided by the membranes and the anchoring of polar groups at the surfaces, the aromatic cores align parallel to the cylinder long axes. This indeed resembles the organization of some T-shaped polyphiles in the hexagonal channeled layer LC phases.[62] We therefore consider the honeycomb model to be the most probable model, although further in-depth characterization of the mesoscale structure will be required for a final conclusion to be drawn.

Conclusion

We demonstrated that a new class of bolapolyphilic molecules exhibited a unique propensity to form supramolecular structures in free-standing lipid bilayer membranes. We found that, as a function of the head-group structure, BPs and lipids reproducibly self-organized in either highly regular, sixfold symmetric structures or less ordered 2D networks. The molecular origin of the three first-order thermal transitions associated with these structures, as seen in DSC, were elucidated by XRD and NMR spectroscopy. By using distinct head groups, it was demonstrated how supramolecular organization could be tuned by molecular design. The mesoscale structure and molecular orientation of **B12** in DPPC and in DMPC have been further investigated by transmission electron microscopy, different X-ray diffraction techniques, fluorescence and polarized infrared spectroscopy, as reported in a separate publication.[51] Because the physical properties of self-assembled materials depend crucially on their supramolecular organization, we envision that a targeted design will enable novel applications in nanotechnology, encapsulation, and drug delivery or template-assisted engineering of scaffolds of π-conjugated rods, which are of interest, for example, for molecular electronics and sensor applications. The investigation of the self-assembly of properly designed synthetic molecules in lipid membranes could also contribute to the better understanding of microdomain formation in biomembranes[4–10] and to the design, stabilization, and investigation of functional membranes and protocells.[63]

Experimental Section

Synthesis

Details of the syntheses and analytical data are described in the Supporting Information.

GUV preparation

The lipid DPPC and red fluorescent lipid marker Rh-PE were purchased from Avanti Polar Lipids (Alabaster, Alabama, USA) and used without further purification. GUVs were prepared by a modified electroformation method.[64,44] With chloroform as a solvent, the DPPC was mixed with one of the BPs at 10:1 molar ratio by adding 0.5 mol% of Rh-PE as a red counterstain. The total concentration was 15 mg mL^{-1}. The mixture (15 μL) was spread on optically transparent indium tin oxide (ITO) coverslips (Gesim GmbH, Grosserkmannsdorf, Germany) preheated to 60°C. The coverslips were assembled in a capacitor-type configuration by using a home-built perfusion chamber with 2 mm spacers. The chamber was filled with deionized water and an alternating sinusoidal voltage (1.3 V effective voltage, 10 Hz) was applied for 4 h at 60°C. Prior to confocal microscopy, the perfusion chamber was allowed to cool to room temperature (22°C).

CFM measurements

CFM was carried out on an LSM 710 setup (Carl Zeiss Microimaging, Jena, Germany) by using a C-Apochromat 40×/1.2 N.A. water immersion objective at room temperature. The BPs were excited with a diode laser at $\lambda = 405$ nm; the fluorescence emission was collected from $\lambda = 412$ to 500 nm by using a photomultiplier detector. A $\lambda = 561$ nm DPSS laser was used to excite the lipid marker Rh-PE; the fluorescence emission of the marker was collected from $\lambda = 566$ to 681 nm. Spectrally resolved confocal imaging was performed on an LSM 780 setup (Carl Zeiss Microimaging, Jena, Germany) by using a C-Apochromat 63×/1.2 N.A. water immersion objective. Fluorescence was collected between $\lambda = 414$ and 690 nm at 8.9 nm resolution by using a 32-channel GaAsP detector. Spectral plots were generated for selected regions of interest (ROIs). For the reference measurement, an image of a solution of **B12** in CHCl$_3$/MeOH (2:1) was acquired and a spectral plot for an arbitrary ROI within the uniform image was generated.

DSC measurements

DSC thermograms were acquired by using a VP-DSC[65] instrument (MicroCal/GE Inc. Northampton, USA) with heating/cooling rates of 60 K h^{-1} in a temperature range of 2–95°C. The traces shown in Figure 5 represent the seventh heating scan of mixed vesicles prepared as follows: All components were mixed in CHCl$_3$/MeOH (2:1) at the required molar ratio; the organic solvent was then evaporated in a stream of N$_2$ to obtain a lipid film. The film was further dried under reduced pressure at 70°C for about 3 h. After hydration with H$_2$O, the sample had a total concentration of 2.0–2.5 mM. The aqueous suspension was then vortexed and sonicated at about 60°C for 30 min to obtain vesicles. All DSC results were reproducible for repeated sample preparations, and showed no significant hystereses, except for the first few heating–cooling cycles, after which the samples were in equilibrium.

XRD measurements

The XRD measurements of lipid mixtures were performed by using monochromic Cu$_{K\alpha1}$ radiation ($\lambda = 0.154051$ nm from a Ge(111)

monochromator (Seifert X-ray/GE Inc. Freiberg) and a curved linear position-sensitive detector (range: $2\theta = 0$–$40°$). Samples were prepared according to the standard procedure followed by lyophilization and rehydration to give a water content of 50 wt% for a good signal to noise ratio of the scattering patterns. The samples were transferred into glass capillaries, which were then flame-sealed. The temperature was controlled by using a high-temperature sample holder (STOE & CIE GmbH, Darmstadt). SAXS and WAXS ($s = 1$–4.7 nm^{-1}) data were collected in the temperature range from -35 to $80°C$. The temperature was varied stepwise (heating rates of 1 K min^{-1}) and the sample was equilibrated for 5 min at each temperature before data acquisition with 10 min of exposure time per diffractogram. Each scattering pattern was corrected by subtracting the scattering of an empty capillary. All diffraction patterns of one temperature series were then converted into a contour diagram (intensities in grayscales).

NMR spectroscopy

Static ^{31}P and MAS ^1H NMR spectroscopy investigations were carried out on MLV preparations made by co-dissolving lipid and **B12** in methanol/chloroform, drying, and subsequent rehydration by adding 50 wt% of H_2O/D_2O to the powder. All data were acquired on a Bruker Avance III instrument with 400 MHz ^1H Larmor frequency by using a Bruker static 5 mm double-resonance probe for ^{31}P spectra and a Bruker 4 mm MAS WVT double-resonance probe head at 5 kHz spinning frequency (if not indicated otherwise) for ^1H spectra, relying in both cases on a flow of heated air for temperature regulation. Typical 90° pulse lengths were 3 μs for both ^{31}P and ^1H NMR spectra.

^{31}P direct-polarization spectra to characterize the motion of the lipid head groups were taken with a 3 s repetition time and ^1H decoupling achieved by using SPINAL64.[66] The ^{31}P NMR chemical shift was calibrated with 85% H_3PO_4 ($\delta = 0$ ppm) as an external reference. In addition, T_2 relaxation time measurements were performed with a standard Hahn-echo sequence ($90°_x - t/2 - 180°_y - t/2 - $acq) with an eight-step phase cycle and ^1H decoupling over the whole sequence. The Fourier-transformed echo signals were integrated within a narrow range around the magic-angle orientation and fitted exponentially. The decoupling strength was adjusted to around 10–30 kHz nutation frequency, which represented a good compromise between sample heating at high power and additional line broadening (T_2 reduction) at low power.

Quantitative ^1H spectra were taken at 5 kHz MAS. Weight-controlled samples were prepared in 4 mm MAS rotors with Teflon spacers for reproducible sample positioning. The recycle delay was adjusted to a value much larger than T_1 at each temperature, and the spectral intensities were corrected for the Curie temperature dependence, by multiplying them by T/T_{ref}, and allowing for a quantitative evaluation of the integrals. The aliphatic, aromatic, and glycerol resonances of DPPC and **B12** in the gel phase (20°C) at the given spinning frequency were subject to dipolar line broadening down to the baseline level due to the well-defined packing and low mobility; this precluded their observation in sufficiently narrow integration ranges. Just above the main lipid phase transition, all resonances of pure hydrated DPPC became well resolved and quantitatively detectable, although their intensity remained lower for the mixtures. The resolved glycerol resonance of the pure DPPC preparation at $T_{ref} = 50°C$ served as an external intensity standard to define 100% of the signal for each group of resonances. Notably, a significant intensity was found in sharp spinning

sidebands, which were also integrated. At 75°C and above, the Curie-corrected integrals did not change further, which indicated that all species were sufficiently mobile. The deviations of this high-temperature data from 100% also demonstrated that the measurements were subject to systematic errors on the order of 20%, which could be explained by baseline problems upon integration, and external calibration, for which a change of the sample in a MAS rotor could lead to setup variations, and thus, deviations in the absolute spectral intensities.

^1H–^1H dipole–dipole coupling constants for the adjacent aromatic CH protons were determined by DQ[57] spinning sideband analysis[58] by using the BaBa-xy16 pulse sequence[55] at 10 kHz MAS and four rotor periods recoupling. The pattern was fitted to a numerically calculated and Fourier-transformed powder average of the theoretical time domain signal by assuming a Gaussian distribution of residual dipole–dipole couplings, D_{res}. The standard deviation was always around 10% of the average, which indicated weak apparent distribution effects.[67] Such effects did not necessarily arise from an actual coupling distribution, but could also be assigned to changes in the pattern shape that arose from couplings to remote protons[58c] or from a bias in the assumed isotropic powder average[57] that arose from anisotropic T_2.

Acknowledgements

[1] D. A. Doyle, *Science* **1998**, *280*, 69–77.
[2] Y. Shai, *Biochim. Biophys. Acta Biomembr.* **1999**, *1462*, 55–70.
[3] N. Sakai, S. Matile, *Langmuir* **2013**, *29*, 9031–9040.
[4] D. A. Brown, E. London, *J. Biol. Chem.* **2000**, *275*, 17221–17224.
[5] K. Simons, W. L. C. Vaz, *Annu. Rev. Biophys. Biomol. Struct.* **2004**, *33*, 269–295.
[6] J. M. Moran-Mirabal, D. M. Auberecht, H. G. Craighead, *Langmuir* **2007**, *23*, 10661–10671.
[7] U. Bernchou, J. H. Ipsen, A. C. Simonsen, *J. Phys. Chem. B* **2009**, *113*, 7170–7177.
[8] K. Simons, M. J. Gerl, *Nat. Rev. Mol. Cell Biol.* **2010**, *11*, 688–699.
[9] R. F. de Almeida, E. Joly, *Front. Plant Sci.* **2014**, *5*, 72
[10] L. A. Bagatolli, J. H. Ipsen, A. C. Simonsen, O. G. Mouritsen, *Prog. Lipid Res.* **2010**, *49*, 378–389.
[11] W. H. Binder, V. Barragan, F. M. Menger, *Angew. Chem. Int. Ed.* **2003**, *42*, 5802–5827; *Angew. Chem.* **2003**, *115*, 5980–6007.
[12] A. Hädicke, A. Blume, *J. Colloid Interface Sci.* **2013**, *407*, 327–338.
[13] M. Schulz, *Angew. Chem. Int. Ed.* **2013**, *52*, 1829–1833; *Angew. Chem.* **2013**, *125*, 1877–1882.
[14] P. Scholtysek, A. Achilles, C.-V. Hoffmann, B.-D. Lechner, A. Meister, C. Tschierske, K. Saalwächter, K. Edwards, A. Blume, *J. Phys. Chem. B* **2012**, *116*, 4871–4878.

[15] J.-H. Fuhrhop, T. Wang, *Chem. Rev.* **2004**, *104*, 2901–2937.
[16] C. C. Forbes, K. M. DiVittorio, B. D. Smith, *J. Am. Chem. Soc.* **2006**, *128*, 9211–9218.
[17] S. Aleandri, A. Casnati, L. Fantuzzi, G. Mancini, G. Rispoli, F. Sansone, *Org. Biomol. Chem.* **2013**, *11*, 4811.
[18] D. P. Brownholland, G. S. Longo, A. V. Struts, M. J. Justice, I. Szleifer, H. I. Petrache, M. F. Brown, D. H. Thompson, *Biophys. J.* **2009**, *97*, 2700–2709.
[19] N. Sakai, J. Mareda, S. Matile, *Acc. Chem. Res.* **2005**, *38*, 79–87.
[20] A. Vargas Jentzsch, A. Hennig, J. Mareda, S. Matile, *Acc. Chem. Res.* **2013**, *46*, 2791–2800.
[21] W. Wang, R. Li, G. W. Gokel, *Chem. Eur. J.* **2009**, *15*, 10543–10553.
[22] J. M. Moszynski, T. M. Fyles, *Org. Biomol. Chem.* **2010**, *8*, 5139–5149.
[23] T. Muraoka, T. Shima, T. Hamada, M. Morita, M. Takagi, K. Kinbara, *Chem. Commun.* **2011**, *47*, 194–196.
[24] E. Quesada, A. U. Acuna, F. Amat-Guerri, *Angew. Chem. Int. Ed.* **2001**, *40*, 2095–2097; *Angew. Chem.* **2001**, *113*, 2153–2155.
[25] J. Nikolaus, S. Czapla, K. Möllnitz, C. T. Höfer, A. Herrmann, P. Wessig, P. Müller, *Biochim. Biophys. Acta Biomembr.* **2011**, *1808*, 2781–2788W.
[26] For previously reported oligo(phenylene ethynylenes) involving hydrophilic groups, see: E. H. Hill, D. Sanchez, D. G. Evans, D. G. Whitten, *Langmuir* **2013**, *29*, 15732–15737; S. R. Bull, L. C. Palmer, N. J. Fry, M. A. Greenfield, B. W. Messmore, T. J. Meade, S. I. Stupp, *J. Am. Chem. Soc.* **2008**, *130*, 2742–2743; B. Erdogan, J. N. Wilson, U. H. F. Bunz, *Macromolecules* **2002**, *35*, 7863–7864; R. L. Phillips, I.-B. Kim, B. E. Carson, B. Tidbeck, Y. Bai, T. L. Lowary, L. M. Tolbert, U. H. F. Bunz, *Macromolecules* **2008**, *41*, 7316–7320; I.-B. Kim, R. Phillips, U. H. F. Bunz, *Macromolecules* **2007**, *40*, 5290–5293.
[27] a) P. Kieffer, M. Prehm, B. Glettner, K. Pelz, U. Baumeister, F. Liu, X. Zeng, G. Ungar, C. Tschierske, *Chem. Commun.* **2008**, 3861–3863; b) F. Liu, R. Kieffer, X. Zeng, K. Pelz, M. Prehm, G. Ungar, C. Tschierske, *Nat. Commun.* **2012**, *3*, 1104.
[28] a) C. Tschierske, *Angew. Chem. Int. Ed.* **2013**, *52*, 8828–8878; *Angew. Chem.* **2013**, *125*, 8992–9047; b) C. Tschierske, C. Nürnberger, H. Ebert, B. Glettner, M. Prehm, F. Liu, X. Zeng, G. Ungar, *Interface Focus* **2012**, *2*, 669–680.
[29] X. B. Zeng, R. Kieffer, B. Glettner, C. Nürnberger, F. Liu, K. Pelz, M. Prehm, U. Baumeister, H. Hahn, H. Lang, G. A. Gehring, C. H. M. Weber, J. K. Hobbs, C. Tschierske, G. Ungar, *Science* **2011**, *331*, 1302–1306.
[30] a) T. Benvegnu, M. Brard, D. Plusquellec, *Current Opinion in Colloid and Interface Science* **2004**, *8*, 469–479; b) A. Meister, A. Blume, *Current Opinion in Colloid & Interface Science* **2007**, *12*, 138–147; Interface Science **2007**, *12*, 138–147.
[31] a) M. Kölbel, T. Beyersdorff, C. Tschierske, S. Diele, J. Kain, *Chem. Eur. J.* **2000**, *6*, 3821–3837; b) B. Glettner, F. Liu, X. Zeng, M. Prehm, U. Baumeister, M. Walker, M. A. Bates, P. Boesecke, G. Ungar, C. Tschierske, *Angew. Chem. Int. Ed.* **2008**, *47*, 9063–9066; *Angew. Chem. Int. Ed.* **2008**, *120*, 9203–9206.
[32] K. Sonogashira, Y. Tohda, N. Nagihara, *Tetrahedron Lett.* **1975**, *16*, 4467–4470.
[33] C. Eaborn, A. R. Thompson, D. R. M. Walton, *J. Chem. Soc. C* **1967**, 1364–1366.
[34] a) W. B. Austin, N. Bilow, W. J. Kelleghan, K. S. Y. Lau, *J. Org. Chem.* **1981**, *46*, 2280–2286; b) D. L. Musso, M. J. Clarke, J. L. Kelley, G. E. Boswell, G. Chen, *Org. Biomol. Chem.* **2003**, *1*, 498–506.
[35] a) T. Vahlenkamp, G. Wegner, *Makromol. Chem. Phys.* **1994**, *195*, 1933–1952; b) A. Fkyerat, G.-M. Dibin, R. Tabacchi, *Helv. Chim. Acta* **1999**, *82*, 1418–1422.
[36] R. Sterzycki, *Synthesis* **1979**, 724–725.
[37] F. Mitzel, S. Fitzgerald, *Chem. Eur. J.* **2003**, *9*, 1233–1241.
[38] a) J. S. Moore, E. J. Weinstein, Z. Wu, *Tetrahedron Lett.* **1991**, *32*, 2465–2466; b) O. Lavastre, O. Laurence, P. H. Dixneuf, *Tetrahedron* **1996**, *52*, 5495–5504.
[39] a) T. D. Nelson, R. D. Crouch, *Synthesis* **1996**, 1031–1069; b) J. Cheng, U. Hacksell, G. D. Daves, *J. Org. Chem.* **1986**, *51*, 3093–3098.
[40] A. Saha, S. Ramakrishnan, *Macromolecules* **2009**, *42*, 4956–4959.

[41] J. Korlach, P. Schwille, W. W. Webb, G. W. Feigenson, *Proc. Natl. Acad. Sci. USA* **1999**, *96*, 8461–8466.
[42] K. Bacia, P. Schwille, T. Kurzchalia, *Proc. Natl. Acad. Sci. USA* **2005**, *102*, 3272–3277.
[43] N. Rodriguez, F. Pincet, S. Cribier, *Colloids Surf. B* **2005**, *42*, 125–130.
[44] M. Schulz, D. Glatte, A. Meister, P. Scholtysek, A. Kerth, A. Blume, K. Bacia, W. H. Binder, *Soft Matter* **2011**, *7*, 8100–8110.
[45] S. L. Veatch, S. L. Keller, *Biophys. J.* **2003**, *84*, 725–726.
[46] X. Y. Liu, From solid-fluid interfacial structure to nucleation kinetics: principles and strategies for micro/nanostructure engineering; in: Xiang Yang Liu, James J. De Yoreo, Nanoscale structure and assembly at solid-fluid interfaces, Vol. 1, Kluwer Academics Publishers **2004**, ISBN 1 4020 7792 0.
[47] J. Yguerabide, L. Stryer, *Proc. Natl. Acad. Sci. USA* **1971**, *68*, 1217–1221.
[48] D. Axelrod, *Biophys. J.* **1979**, *26*, 557–574.
[49] R. R. Gullapalli, M. C. Demirel, P. J. Butler, *Phys. Chem. Chem. Phys.* **2008**, *10*, 3548–3560.
[50] J. F. Nagle, S. Tristram-Nagle, *Biochim. Biophys. Acta Rev. Biomembr.* **2000**, *1469*, 159–195.
[51] B.-D. Lechner, H. Ebert, M. Prehm, S. Werner, A. Meister, G. Hause, A. Beerlink, K. Saalwächter, K. Bacia, C. Tschierske, A. Blume, *Langmuir* **2015**, *31*, 2839–2850.
[52] G. Förster, A. Meister, A. Blume, *Current Opinion in Colloid & Interface Science* **2001**, *6*, 294–302; Interface Science **2001**, *6*, 294–302.
[53] J. Seelig, *Biochim. Biophys. Acta Rev. Biomembr.* **1978**, *515*, 105–140.
[54] E. J. Dufourc, C. Mayer, J. Stohrer, G. Althoff, G. Kothe, *Biophys. J.* **1992**, *61*, 42–57.
[55] a) K. Saalwächter, F. Lange, K. Matyjaszewski, C.-F. Huang, R. Graf, *J. Magn. Reson.* **2011**, *212*, 204–215; b) M. Feike, D. E. Demco, R. Graf, J. Gottwald, S. Hafner, H. W. Spiess, *J. Magn. Reson. Ser. A* **1996**, *122*, 214–221.
[56] D. Reichert, K. Saalwächter in *NMR Crystallography (Encyc. Magn. Reson.)*, (Eds.: R. K. Harris, R. E. Wasylichen, M. J. Duer), Wiley, Chichester **2009**, pp. 177–193.
[57] K. Saalwächter, *ChemPhysChem* **2013**, *14*, 3000–3014.
[58] a) R. Graf, D. E. Demco, J. Gottwald, S. Hafner, H. W. Spiess, *J. Chem. Phys.* **1997**, *106*, 885–895; b) I. Schnell, S. P. Brown, H. Y. Low, H. Ishida, H. W. Spiess, *J. Am. Chem. Soc.* **1998**, *120*, 11784–11795; c) I. Schnell, H. W. Spiess, *J. Magn. Reson.* **2001**, *151*, 153–227.
[59] I. Fischbach, T. Pakula, P. Minkin, A. Fechtenkötter, K. Müllen, H. W. Spiess, K. Saalwächter, *J. Phys. Chem. B* **2002**, *106*, 6408–6418.
[60] T. Rudolph, N. K. Allampally, G. Fernandez, F. H. Schacher, *Chem. Eur. J.* **2014**, *20*, 13871–13875.
[61] a) B. Chen, X. Zeng, U. Baumeister, G. Ungar, C. Tschierske, *Science* **2005**, *307*, 96–99; b) C. Tschierske, *Chem. Soc. Rev.* **2007**, *36*, 1930–1970.
[62] a) B. Chen, X. Zeng, U. Baumeister, S. Diele, G. Ungar, C. Tschierske, *Angew. Chem. Int. Ed.* **2004**, *43*, 4621–4625; *Angew. Chem.* **2004**, *116*, 4721–4725; b) B. Chen, U. Baumeister, G. Pelzl, M. K. Das, X, Zeng, G. Ungar, C. Tschierske, *J. Am. Chem. Soc.* **2005**, *127*, 16578–16591 .
[63] S. Rasmussen, M. A. Bedau, L. Chen, D. Deamer, D. C. Krakauer, N. H. Packard, P. F. Stadler, *Protocells: Bridging Nonliving and Living Matter*, MIT Press, Cambridge, MA, **2009**.
[64] M. I. Angelova, D. S. Dimitrov, *Faraday Discuss. Chem. Soc.* **1986**, *81*, 303–311.
[65] V. V. Plotnikov, J. M. Brandts, L. N. Lin, J. F. Brandts, *Anal. Biochem.* **1997**, *250*, 237–244.
[66] B. M. Fung, A. K. Khitrin, K. Ermolaev, *J. Magn. Reson.* **2000**, *142*, 97–101.
[67] a) S. P. Brown, I. Schnell, J. D. Brand, K. Müllen, H. W. Spiess, *J. Mol. Struct.* **2000**, *521*, 179–195; b) G. P. Holland, B. R. Cherry, T. M. Alam, *J. Magn. Reson.* **2004**, *167*, 161–167.